OBSERVATIONS OF THE MARS POLAR VORTEX WITH THE MARS EXPRESS PLANETARY FOURIER SPECTROMETER. M. Giuranna[1], V. Formisano[1], L. Montabone[2], G. Rinaldi[1]
[1]IFSI-INAF, Rome, Italy, marco.giuranna@ifsi-roma.inaf.it; [2]Department of Physics & Astronomy, The Open University, Walton Hall, United Kingdom, montabone@atm.ox.ac.uk

Introduction: Polar vortices are of interest because they act as a barrier, inhibiting energy transport and potentially preventing the mixing of aerosols and chemical species. Thus, they control the response of winter polar processes to climatic forcing, both short and long term. On Mars, the polar jet support stationary and travelling waves of zonal wave numbers 1, 2 and 3, with most of the amplitude in zonal wave number 1. Another concern, unique to Mars, is that CO2 condensation is a dynamically important process. Recent observations suggest that CO2 condensate clouds are pervasive inside the polar vortex. For this reason, comparisons between atmospheric temperatures and CO2 saturation curves are extremely important.

The Mars Express (MEX) Planetary Fourier Spectrometer (PFS) data set provides several Martian years of consistently sampled, vertically resolved temperature measurements, allowing us to take a detailed look at the different aspects and behaviours exhibited by the Mars polar vortex. We present our methodology for the computation of winds and potential vorticity, and some preliminary results.

METHODOLOGY

PFS temperature retrievals: We start with MEX-PFS retrievals of temperature as a function of pressure. Typical quality of modeling for temperature retrievals is shown in Fig. 1.

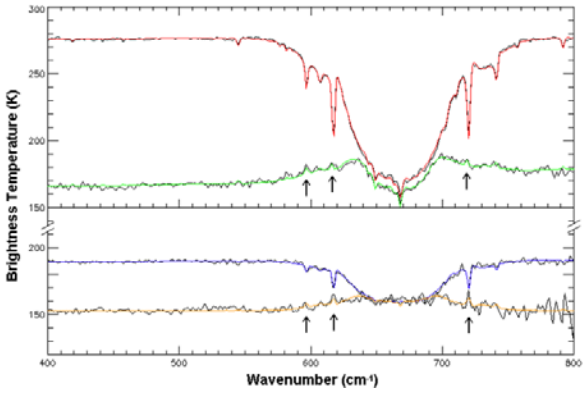

Fig. 1 Typical quality of PFS spectra modeling for different thermal conditions of the atmosphere. Black curves: single spectra measured by PFS. Colored curves: synthetic. Black arrows indicate the CO_2 Q-branches.

In consideration of the intrinsically limited resolution of these measurements, and in order to prevent our working data set from becoming unmanageably large, we sample the derived temperature profiles at intervals of one-quarter scale height. Our data set is limited to the lowest five scale heights of the atmosphere. We have used only PFS nadir-pointed observations for the work presented here. Noteworthy, the high spectral resolution of PFS allows the detection of several different thermal gradients in the atmosphere, as demonstrated by the effective modeling in the same spectrum of absorbing and emitting Q-branches (see Fig. 1).

Temperature analysis grid: In order to support the calculation of dynamically important quantities such as winds and potential vorticity, we interpolate the PFS temperature retrievals onto grids with uniform sampling in latitude (1°), longitude (10°), and altitude in log-pressure coordinates (one-quarter scale heoght). An example of gridded sataset for the range of L_S 0°-15° is provided in Fig. 2

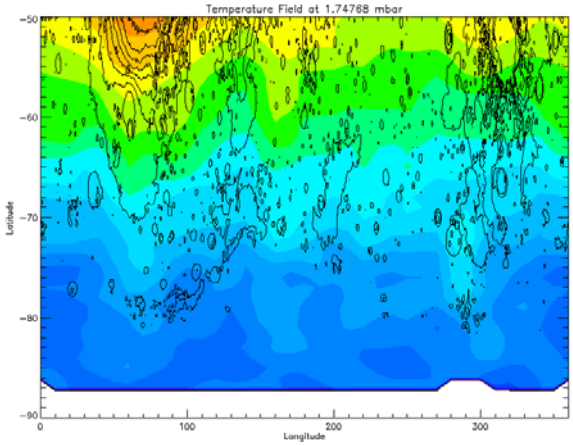

Fig. 2 Thermal field at 1.75 mbar after gridding and interpolation for "morning" observations in the 0°-15° LS range. Surface altimetry (black contours) is shown for -8 km < h < -1 km. Temperatures range from 80 K (blue) to 198 K (orange).

We generate one set of grids for the "morning" temperatures, and another set for the "evening" temperatures. Since all of the source measurements are for same local solar time, each grid obviously contains none of the diurnal variation that would exist in a true instantaneous measurement of global temperatures. In

other words, our analysis grids are maps of instantaneous morning (or evening) temperatures with the diurnal component "removed." At each grid latitude, and for each pressure level, the temperature is determined from weighted average of neighboring data point temperatures.

The weight Wn of the n-th data point is given by a 2-dimensional gaussian function of latitude (FWHM=1°) and longitude (FWHM=10°). A linear interpolation of the temperatures in all available orbits within a selected range of LS is performed to map them onto grid longitudes. If the gap in longitude between adjacent points is larger than 70°, then all the temperatures that fall between these points are considered to be missing.

Geopotential Height: We assume hydrostatic equilibrium in order to calculate the geopotential height Z_{ijk} at each grid latitude ϕ_j, longitude λ_i and pressure level p_k, above some reference pressure level, $p = p\ (k_{ref})$, by vertical integration of the temperature field.

$$Z_{ijk} = \frac{\Delta_{\ln p}}{2}\frac{R}{g_0}\sum_{k'=k_{ref}+1}^{k}\left(T_{ijk'} + T_{ij(k'-1)}\right)$$

R is the specific gas constant, and g_0 is the surface gravity. Δ_{lnp} is the vertical grid spacing (which is a constant in log-pressure coordinates). We treat the geopotential height as a constant at $k = k_{ref}$ and arbitrarily define $Z_{ijkref} = 0$.

Since the main purpose of our geopotential height calculations is to facilitate subsequent calculation of winds, this constant geopotential assumption is essentially equivalent to the usual assumption of zero wind at some reference pressure level. We have chosen $k_{ref} = 1$. Given our grid specifications $p(k_{ref}) = 3.70$ mb.

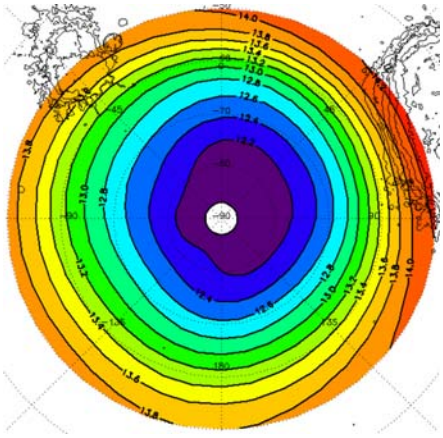

Fig. 3 Geopotential Height at 0.83 mb (L_S 0°-15°)

If, at a certain i and j, a T_{kref} is missing then, for purposes of calculating Z_k, T_{kref} is found by linear extrapolation of T from the two lowest non-missing T_k. This extrapolation is necessary to prevent persistent data gaps at or near the locations of topographic highs. If there are fewer than 2 points at the given i and j with $k \geq k_{ref}$, then all of the Z_k at that i and j are considered to be "missing".

Non-linear Balance Winds: We calculate horizontal winds from the geopential height data using a variation of the non-linear balance wind method suggested by [1]. This method seeks an approximate solution to the full primitive equations for zonal and meridional momentum balance, neglecting only the local time derivatives and the vertical wind components. We generate wind estimates for latitudes poleward of ±45°. The calculation is performed separately for each pole.

The balance equations are:

$$\varepsilon_u = u + \frac{g_0}{af}\frac{\partial z}{\partial \phi} + \frac{1}{af}v\frac{\partial v}{\partial \phi} + \frac{\tan\phi}{af}u^2 + \frac{1}{af\cos\phi}u\frac{\partial v}{\partial \lambda}$$

$$\varepsilon_v = v - \frac{g_0}{af\cos\phi}\frac{\partial z}{\partial \lambda} - \frac{1}{af\cos\phi}u\frac{\partial u}{\partial \lambda} + \frac{\tan\phi}{af}uv - \frac{1}{af}v\frac{\partial u}{\partial \varphi}$$

where f is the coriolis parameter, $f = 2\Omega\sin f$, a is the radius of Mars, Ω is the angular velocity of Mars about its rotation axis, u is the eastward wind component, and v is the northward wind component.

An exact solution to the balance equations would have $\varepsilon_u = 0$ and $\varepsilon_v = 0$. However, an exact solution does not in general exists, and we therefore seek an approximate solution for the u and v fields that minimizes the ε_u and ε_v fields in a root-mean-square sense. In order to converge on a solution for u and v, we found it necessary to include smoothing in the horizontal spatial dimensions as part of the algorithm. This is accomplished by convolution with a gaussian kernel, S:

$$S_{ij} = \begin{cases} e^{-\left(\frac{i^2}{2\sigma_{lat}^2}\right)} \cdot e^{-\left(\frac{j^2}{2\sigma_{lon}^2}\right)} & \text{if } -3\sigma_{lat} \leq i \leq 3\sigma_{lat} \text{ and } -3\sigma_{lon} \leq i \leq 3\sigma_{lon} \\ 0 & \text{otherwise} \end{cases}$$

σ_{lat} and σ_{lon} are chosen such that the FWHM of the gaussian in that dimension is equal to 5° and 50° respectively.

Prior to the start of the wind-finding algorithm, the geopotential height grid at each pressure level is smoothed according to S_{ij}, and the smoothed Z values are used at all stages of the algorithm. All of the operations involved in the algorithm are performed

simultaneously on each pressure level, so that the final result at each level is based on the same number of iterations.

The initial guess for the wind solution is the gradient wind for the *u* component, and geostrophic for the *v* component.

$$u = -\Omega a\cos\phi + \sqrt{(\Omega a\cos\phi)^2 - \frac{g_0}{\tan\phi}\frac{\partial Z}{\partial\phi}}$$

$$v = \frac{g_0}{af\cos\phi}\frac{\partial Z}{\partial\lambda}$$

Examples of wind fields calculated with the method discussed above are shown in Fig. 4. Integrated dust and ice content are shown in Fig. 5.

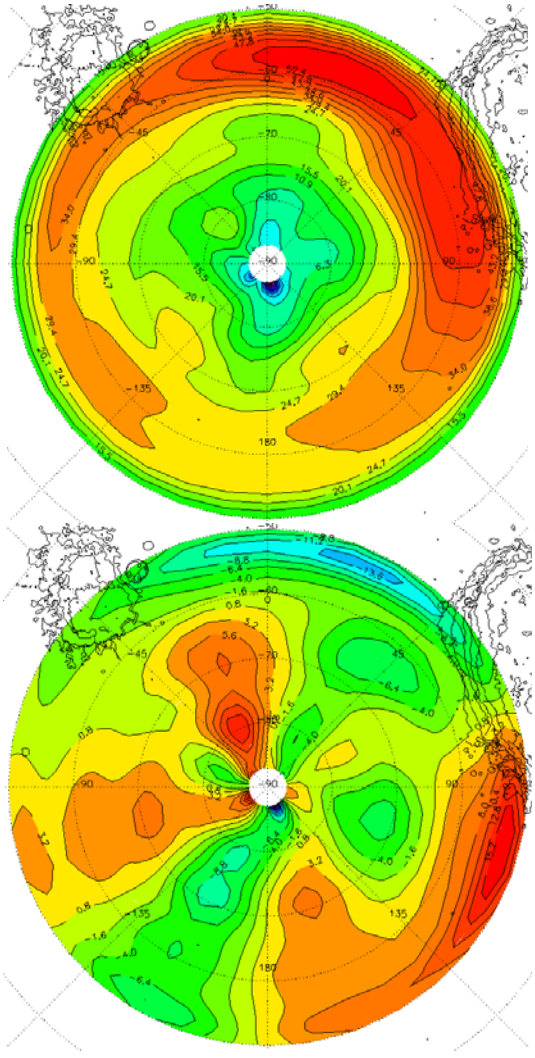

Fig. 4 L_S 0°-15°. *Top*: Eastward wind fields *u* at 0.83 mbar. *Bottom*: Northward wind fields *v* at 0.83 mbar.

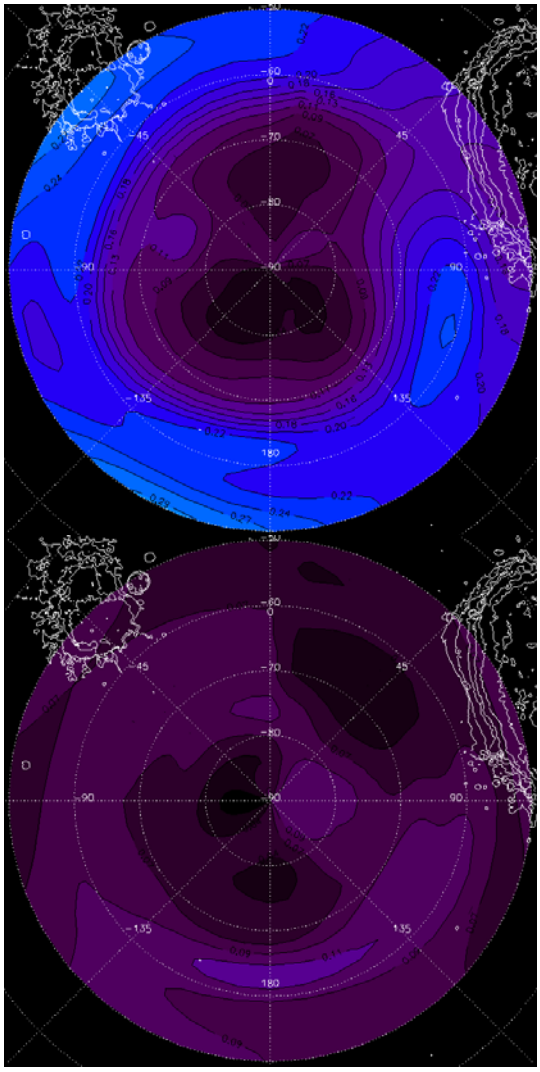

Fig. 5 L_S 0°-15°. *Top*: Integrated dust content. *Bottom*: Integrated water ice content.

Ertel Potential Vorticity: Ertel potential vorticity, *PV*, is defined in an intertial frame as:

$$PV = \frac{\left(\vec{\nabla}\times\vec{v}\right)\cdot\vec{\nabla}\theta}{\rho}$$

where *v* is the velocity vector and *r* is the density

Potential temperature, θ: We calculate PV in the co-rotating, log-pressure coordinate system of our analysis grid. We define θ relative to the 6.1mb pressure level on Mars. We assume that C_p is approximately constant for the lower atmosphere of Mars (T_{mean} = 210 K).

$$\theta = T\left(\frac{6.1mb}{p}\right)^{\frac{R}{c_p}}$$

In order to show PV on θ coordinate surfaces, we apply a linear interpolation from the PV on log-pressure surfaces onto the desired θ coordinate surface using the θ values calculated for each grid point.

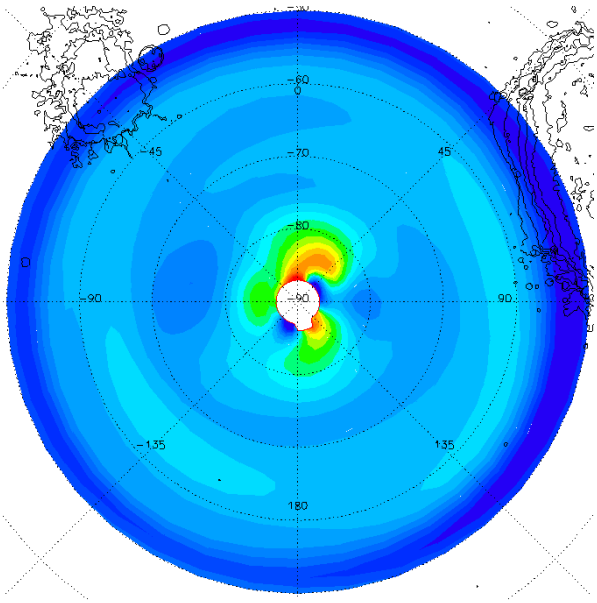

Fig. 6 PV on the θ = 240 K surface (LS 35°-55°).

References: [1] Randel, W. J., 1987. The Evaluation of Winds from Geopotential Height Data in the Stratosphere. Journal of Atmospheric Sciences 44, 3097–3120.